



Integrated geophysical investigation for understanding agriculturally induced landslides in southern Peru

Hanna E. Flamme¹ · Richard A. Krahenbuhl¹ · Yaoguo Li¹ · Brandon Dugan^{1,2} · Jeffrey Shragge¹ · Andrew Graber³ · Dana Sirota¹ · Gavin Wilson¹ · Edgard Gonzales⁴ · Javier Ticona⁴ · Armando Minaya⁴

Received: 16 June 2021 / Accepted: 3 April 2022 / Published online: 26 May 2022
© The Author(s) 2022

Abstract

We conducted near-surface geophysical surveys in and around the Majes I agricultural development (60 km west of Arequipa, Peru), where the nexus of geology and agriculture has increased landslide activity along the Majes–Sigüas River Valley. Through DC resistivity, transient electromagnetics (TEM), and seismic surveys, we refined the understanding of local geology, characterized the agricultural impact on the local water table, and updated landslide modeling to help inform discussions on landslide mitigation strategies at Majes I and landslide prevention at the planned Majes II site. At the Majes I development, we identified an increase in water table and water saturation due to irrigation. At the planned Majes II site, which shares similar geology to Majes I, we interpret the regional water table that has yet to be affected by significant human development. We integrated these results into updated landslide modeling. Our modeling for Majes I suggests stable conditions prior to irrigation; as the water table rose from irrigation, landsliding began and evolved as a retrogressive failure that is now focused along the headscarp near critical infrastructure including the Carretera Panamericana (Pan-American Highway). Majes II is currently stable and irrigation management, such as drip versus flood techniques, must be supported. Soil ameliorants such as polymers and/or biochar should be encouraged to hold water near the roots to reduce the risk of landslide initiation. Combined this work shows the value of integrated hydrological and geophysical research for landslide management and optimized irrigation.

Keywords Geophysics · Landslide · Agriculture · Modeling · Aquifer · Peru

Introduction

Majes is one of the largest and most important agricultural developments in the Arequipa region of southern Peru (Fig. 1). The agricultural development was established along the north–west ridge of the Sigüas River Valley in the early 1980s atop one of the broad coastal plateaus, referred to as pampas, and it includes approximately 160 km² of irrigated

land in an arid environment (Wei et al. 2021). The Majes development provides agricultural commodities to the surrounding region and contributes over US-\$800 million to the Peruvian GDP per year (Gobierno Regional Arequipa 2016).

To prepare for such a significant agricultural community in elevated desert plateaus, the Peruvian government began the construction of the Majes–Sigüas irrigation project in 1971 to transport large volumes of water to the region. The irrigation project is one of the largest civil works in southern Peru, transporting approximately 34 m³/s of water over 100 km of aqueduct starting at Rio Colca and ending at the Sigüas River (Gobierno Regional Arequipa 2016). From the Sigüas River, water is moved through 16 km of canal to the Pampa de Majes, where it provides year-round support for agricultural crops including avocado, corn, onion, grapes, tomato, garlic, green beans, pepper, potato, paprika, and alfalfa (Huanca 2011; Gobierno Regional Arequipa 2016). Following the success of agricultural development at Majes I, the Majes–Sigüas irrigation project soon will be expanded

✉ Hanna E. Flamme
hflamme@mines.edu

¹ Department of Geophysics, Colorado School of Mines, Golden, CO 80401, USA

² Hydrologic Science and Engineering Program, Colorado School of Mines, Golden, CO 80401, USA

³ Department of Geology and Geological Engineering, Colorado School of Mines, Golden, CO 80401, USA

⁴ School of Geophysical Engineering, Universidad Nacional de San Agustín de Arequipa, Arequipa, Peru

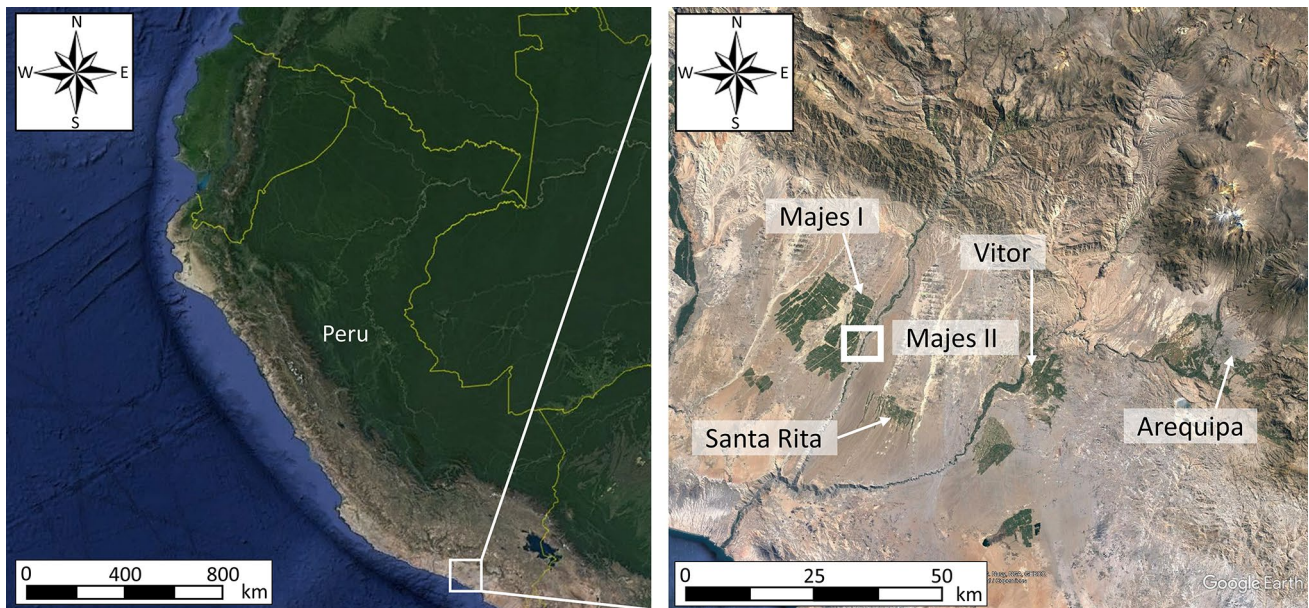


Fig. 1 Location of the Majes I and the planned Majes II agricultural sites in southern Peru. The development is approximately 60 km west of Arequipa and 50 km north–east of the Pacific Ocean. The white box indicates the location of the primary landslide (El Zarzal) and the

geophysical surveys performed at the site. Images taken from Google Earth: Copyright 2021 Google, Image Copyright 2021 CNES/Airbus, Image Copyright 2021 Maxar Technologies

to open an additional 460 km² of land for agricultural development along the neighboring pampa to the south–east of the Sigwas River Valley. This expanded project is known as the Majes–Sigwas II irrigation project, and once completed the new agricultural site will adopt the name Majes II (Gobierno Regional Arequipa 2016).

While the development of Majes I has brought numerous benefits including contribution to local and global food supply and job creation, it has also altered the local hydrology, which in turn has resulted in an increase in landslide activity and occasional damming of the Sigwas River (Gobierno Regional Arequipa 2016). Such unintended consequences from agricultural development are not unique to southern Peru, but are in fact a significant and well recognized issue around the world (Garcia-Chevesich et al. 2021). For example, in the Gansu Province of China, intensive irrigation practices began along the Heifangtai loess platform following dam construction along the Yellow River and the subsequent re-settlement of thousands of farmers (Wu et al. 1999). These agricultural activities saturated the near surface, increased the elevation of the perched water table, and triggered thousands of mass movements and landslides in the area (Lee et al. 2008; Jin and Dai 2007; Dong et al. 2013). While the backstory, geology, and environment varies from site to site, similar observations of agriculturally induced landslides can be found in many other countries including: Argentina (Jurio et al. 2014), Ecuador (Yadún et al.

2020), Nicaragua (Rosales and Centeno 2009), Honduras (Reyes et al. 2006), Costa Rica (Carbajal 2019), Indonesia (Bradley et al. 2019), United States (Knott 2008), Canada (Clague and Evans 2003), Uganda (Gorokhovich et al. 2012), Russia (Ishihara et al. 1990), Pakistan (Ali et al. 2017), and elsewhere in Peru (Lacroix et al. 2020; Araujo-Huamán et al. 2017; Valderrama et al. 2015; Soncco and Manrique 2018). A comprehensive review of agriculturally induced landslides from around the world can be found in Garcia-Chevesich et al. (2021).

Geophysics has a long and well established history for imaging geology and for monitoring active landslide areas around the world. Hussain et al. (2019) performed a combination of seismic, resistivity, and ground penetrating radar surveys to successfully identify the primary slip surface of the Sobradinho landslide in Brazil. Mainsant et al. (2012) used ambient seismic information for failure prediction of the Bourquin clay landslide in the Swiss Alps. Helmstetter and Garambois (2010) correlated seismic signals with rainfall to monitor the Séchilienne rockslide in the French Alps. In Italy, Perrone et al. (2004) used electrical resistivity tomography (ERT) to identify the resistivity contrast associated with the mobilized body of the Varco d’Izzo landslide. In North Yorkshire (United Kingdom), Chambers et al. (2011) deployed an ERT array for automated 3D and 4D landslide monitoring with near-real time measurements. In Peru, Best et al. (2009) used DC resistivity, electromagnetics, and ground penetrating radar to map fractures and zones

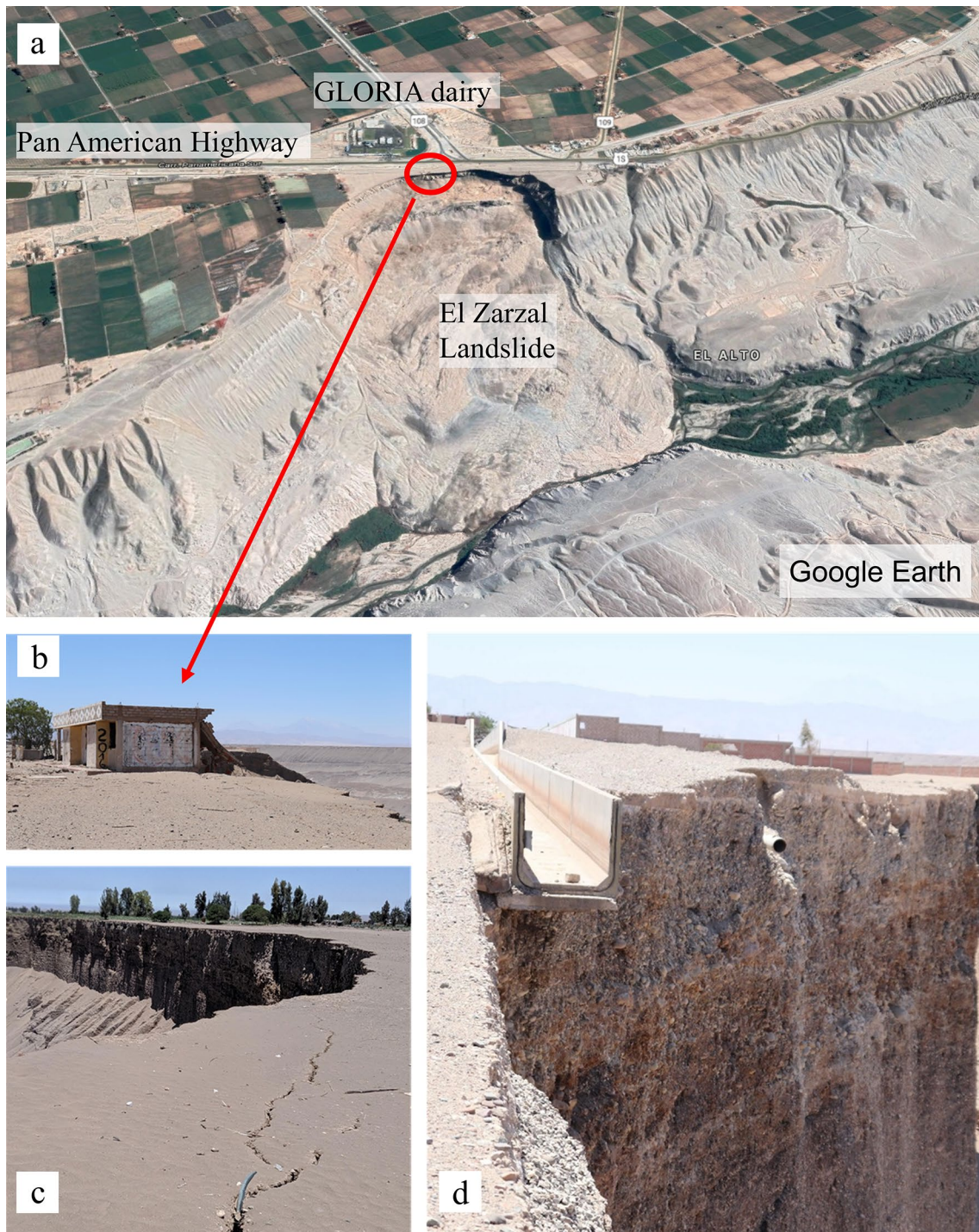


Fig. 2 El Zarzal landslide. **a** Aerial view of the landslide showing the location relative to the Pan-American Highway and GLORIA dairy facility. **b** Abandoned structure on the edge of the scarp. **c** Crown

fractures along the edge of the scarp. **d** Abandoned canal from landslide progression and a view of the poorly consolidated Millo conglomerates

of weakness in the crystalline bedrock at the UNESCO World Heritage site of Machu Picchu.

We focus on the Majes region as the combination of the geology and irrigation for agriculture is increasing landslide activity along the north–west wall of the Sigwas River valley.

Of greatest importance is the El Zarzal landslide (Fig. 2), which is retreating rapidly towards the Carretera Panamericana (Pan-American Highway), GLORIA dairy facility, and numerous agricultural fields. El Zarzal is a slow-moving, retrogressive, complex landslide with activity observable daily.

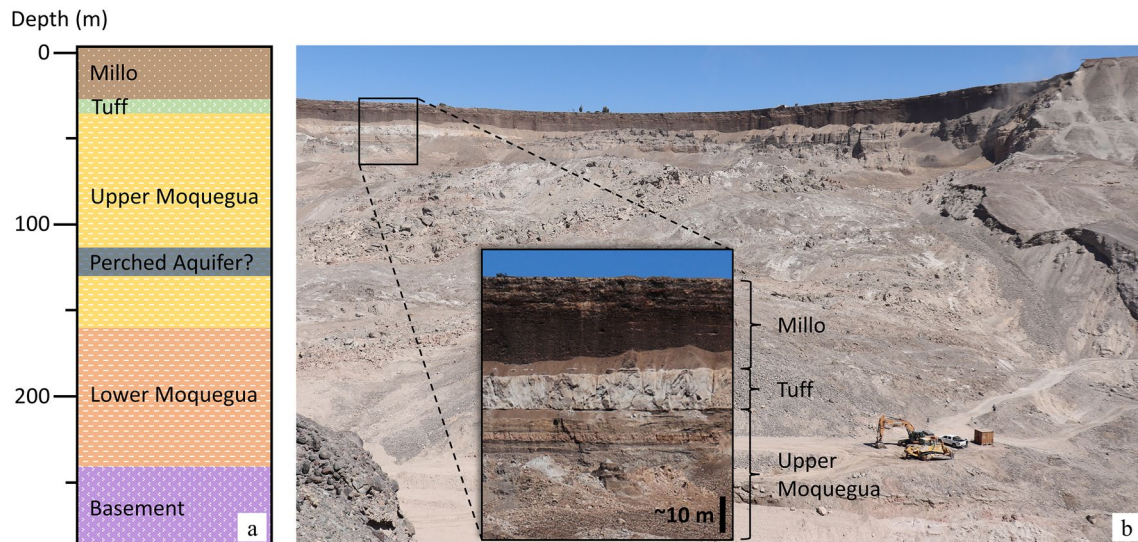


Fig. 3 Initial understanding of geology beneath the Pampa de Majes and El Zarzal landslide. **a** Stratigraphic section showing the significant geologic formations and a possible perched water table to be

investigated (inspired from Meza Arestegui and Chacon Arcaya 2017; Graber et al. 2021). **b** Geological photograph of the stratigraphic section at El Zarzal (photographs taken by H. Flamme)

Local industries and infrastructure are located approximately 100 m from the edge of El Zarzal (Fig. 2). If its retrogressive failure cannot be mitigated, it will soon damage or destroy this infrastructure resulting in excessive social and economic damage for the region.

To start addressing mitigation strategies, we provide a holistic overview of the hydrological and geological conditions in the area. We begin with a brief overview of the relevant geology at Majes, the timing of irrigation onset at the agricultural development, and the history of the primary landslide, El Zarzal. We then summarize our geophysical surveys and interpretations in and around Majes to refine our understanding of the geology and the groundwater system. We use our refined geological and hydrogeological interpretations to update modeling for El Zarzal landslide. We conclude with a discussion on possible mitigation strategies at Majes I and prevention at the planned Majes II site.

Study region

The Majes I and the planned Majes II developments are located in a high desert environment and receive an average of 17 mm of rain per year (Wei et al. 2021). With such limited rainfall in this arid setting, water is provided from the Rio Colca through a series of aqueducts and canals. While landslide activity occurs naturally along the Sigvas Valley walls, the region has seen a marked increase in activity since the onset of irrigation (Lacroix et al. 2020; Graber et al. 2020, 2021).

El Zarzal

Following the completion of the Majes–Sigvas irrigation project, irrigation at Majes began in 1983. In 1996, the first water seepage began to appear along the slopes of what is now El Zarzal slide. In 2004, seepage was observed at the foot of the slope of El Zarzal area, and by 2005 the landslide activity initiated. Since that onset of slip at El Zarzal, fractures have formed along the Pampa de Majes parallel to the main scarp and failures at the foot of the slide have dammed the Sigvas River to create a lagoon. Retrogressive failure of the landslide continues to this day.

Geology at Majes

The near-surface lithology (see Fig. 3) is composed of a sequence of poorly consolidated sediments, including conglomerates, and ignimbritic tuff (Araujo-Huamán et al. 2017). The agricultural development at Majes I is underlain by the Millo conglomerate with an initial estimated thickness of 20–30 m. Within the Millo is a discontinuous layer of tuff of variable thickness. Beneath the Millo lie the Upper and Lower Moquegua Formations with thicknesses estimated around 120 m and 80 m, respectively. The Upper Moquegua Formation consists of sandstones and limonite gravels, whereas the Lower Moquegua is made up of claystones and siltstones.



Fig. 4 Photograph of partially saturated rock along a portion of the Sigwas Valley wall beneath Majes. Photograph taken by H. Flamme and modified from Flamme et al. (2020)

Hydrogeology at Majes

It is believed that water from agricultural irrigation at Majes is percolating through the Millo formation, altering the local water table, and contributing to El Zarzal's recurrent slide activity (Graber et al. 2021). Partially saturated rocks are visible on cliff faces in the Sigwas Valley (Fig. 4) indicating the presence of water within the Upper Moquegua Formation. The Upper Moquegua Formation is generally competent but likely less stable when fully saturated. Thus, detailed characterization and understanding of the groundwater table and its role in landslide evolution is important.

Geophysical surveys

The goals of the geophysical investigation in and around Majes were: (1) to refine our understanding of geology beneath Majes (Fig. 3); (2) to identify the depth of the water table beneath Majes (Figs. 3, 4); and (3) to use this refined information to update modeling of El Zarzal landslide to help inform discussions on possible mitigation at Majes I and prevention at the planned Majes II site. To address the three goals of the project, we performed focused 1D and 2D

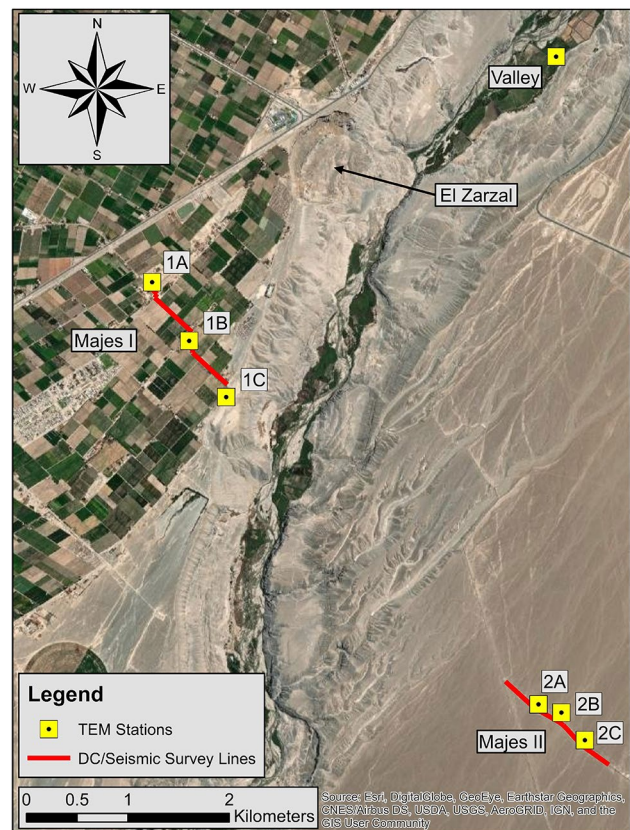


Fig. 5 Survey map from the geophysical field campaign. 2D profiles were performed with DC resistivity and seismic methods in-line and across the valley to capture similar geology with (Majes I) and without (Majes II) the influence of irrigation. TEM soundings were acquired along the survey lines and within the valley floor to help refine the water table and depth to the basement

geophysical surveys at Majes I, Majes II, and on the Sigwas Valley floor. The geophysical field work was conducted 12–19 December 2019.

We targeted Majes I to understand the effects of irrigation; Majes II serves as a reference or control site. We refer to these two survey transects as the Majes I and Majes II lines (Fig. 5). The Majes I and Majes II survey lines were selected with the goal of being approximately in-line while on opposite sides of the valley. A combination of 2D DC resistivity and seismic surveys along with TEM soundings were performed along each line.

Resistivity surveys

Resistivity surveys were performed with an ABEM Terrameter LS-2 (GuidelineGeo) with 64 electrodes and an electrode separation of 20 m providing a total line length of 1260 m (Fig. 5). All surveys were completed with a dipole–dipole configuration. At Majes II, the line was straight. In contrast, at Majes I the survey line was restricted to established dirt

roads and property boundaries and the final survey line contained two bends at approximately 500 m from the Sigvas Valley cliff. Because both lines involve placing electrodes in the upper layer of an arid desert environment, contact resistance was high and the standard practice of adding water to the electrodes was performed where necessary.

Transient electromagnetic (TEM) soundings

Three TEM soundings were performed along the Majes I and Majes II survey lines (Fig. 5). At Majes I, the soundings were typically performed within agricultural fields as approved by local property owners. Data were acquired with an ABEM WalkTEM-1 (GuidelineGeo) with a 40 m × 40 m square transmitter loop with two receivers (10 m × 10 m and 0.5 m × 0.5 m square receiver loop) for dual moment measurement with multiple receiver channels.

Reflection seismic surveys

The seismic data were acquired using a 72-channel Geometrics Geode system consisting of one 24-channel array and six 8-channel strings. The 10 Hz geophones were spaced at 10 m intervals (710 m total array) such that the array half-length of 305 m was roughly equal to the maximum depth of investigation (250–300 m). The team organized the rental of an accelerated weight-drop source that would allow for high repeatability when stacking between five to nine times per shot point. However, due to challenges of importing this piece of equipment, we were required to devise a more creative option for generating source energy that involve hiring a local backhoe operator for 5 days and using the heavy-lifting equipment to raise and drop a heavy rock weight attached to a network of chains. While the backhoe generated a significant amount of source energy, there were several key challenges with source timing, multiple impacts, variable source spectra, and time per shot.

Geophysical results and interpretation

DC resistivity

The two lines of DC resistivity data (Fig. 5) were inverted using a Tikhonov regularization approach assuming a 2D geology (Oldenburg and Li 1994). We used a consistent Chi-square misfit value determined through multiple inversions to be the actual noise level when assuming the standard deviation given by the repeatability of the data. The surface topography, which varies on the order of 5 m at Majes I and 3 m at Majes II, was incorporated into the inversions and the resultant resistivity models are plotted with cut-offs for indicating the depth of investigation as defined by

Oldenburg and Li (1999). The inversion results for Majes II are presented in Fig. 6a, imaging geology without agricultural irrigation, and for Majes I (Fig. 6b) representing geology with irrigation. The bend in the Majes I survey line is identified within Fig. 6b and interpretation within that segment should be considered locally erroneous. Results from the resistivity surveys indicate that the two sites have similar background geology. There is a highly resistive upper layer consistent with the poorly consolidated conglomerates of the Millo formation. This layer is approximately 50 m thick. Beneath the Millo, there is no clear distinction between the Upper and Lower Moquegua formations in either resistivity section; however, it should be noted the predicted depth of investigation for the two surveys (Fig. 6) is at the approximate depth predicted for the contact between the Upper and Lower Moquegua formations (Fig. 3). Finally, and of particular interest, is a distinct decrease in resistivity (increased conductivity) observed at Majes I versus Majes II between approximately 50 m and 100 m depth below the surface. This conductive sequence is consistent with the geologic interpretation and field observations of a saturated zone from irrigation water (Fig. 4) located within the Upper Moquegua formation.

TEM soundings

The TEM sounding data are interpreted using the SPIA TEM processing and inversion software developed by Aarhus GeoSoftware (AGS 2021). Inversions are performed via Gauss–Newton minimization with a Marquardt modification to find the resistivities and thicknesses that minimize the L_2 misfit with respect to the observed data (Auken and Christiansen 2004). The TEM-determined resistivities (Fig. 7) are consistent with the 2D sections recovered from the DC resistivity data (Fig. 6). Results for the TEM sounding along the Sigvas Valley floor indicate a conductive zone (~8 Ohm-m) at a depth of around 160 m below the top of the Pampa de Majes (Fig. 7a). This conductive layer is interpreted as the natural water table and provides a reference value for the resistivity of the fully saturated portion of the Moquegua Formation. The TEM sounding along the Sigvas Valley floor also reveals a transition to a highly resistive layer approximately 220 m depth below the top of the Pampa de Majes. This layer is interpreted as basement. At Majes II, the decrease in resistivity values with depth is attributed to an increase in natural water saturation rather than lithologic changes. The conductive zone (~6 Ohm-m) at approximately 150 m depth below the top of the Pampa de Majes (Fig. 7b) is interpreted as the natural water table with resistivity similar to the saturated zone below of the Sigvas Valley floor. For Majes IA and IB, the Moquegua formation has resistivity near 3 Ohm-m from 85 to 145 m depth below the top of the Pampa de Majes (Fig. 7b), which we interpret to reflect

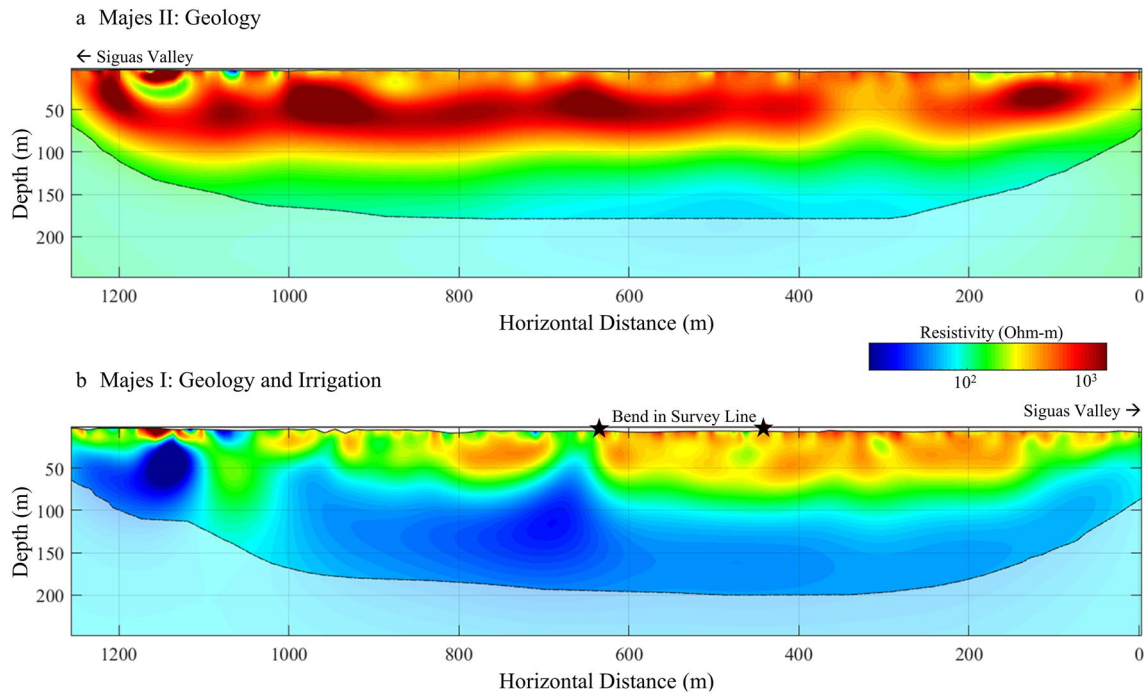


Fig. 6 Geophysical inversion results for electrical resistivity data collected at **a** Majes II and **b** Majes I. The geology is assumed to be similar at both sites. The primary differences in electrical resistivity

are, therefore, associated with the infiltration of agricultural water and raising of the local water table (Fig. 4). Survey line and station locations are shown in Fig. 5

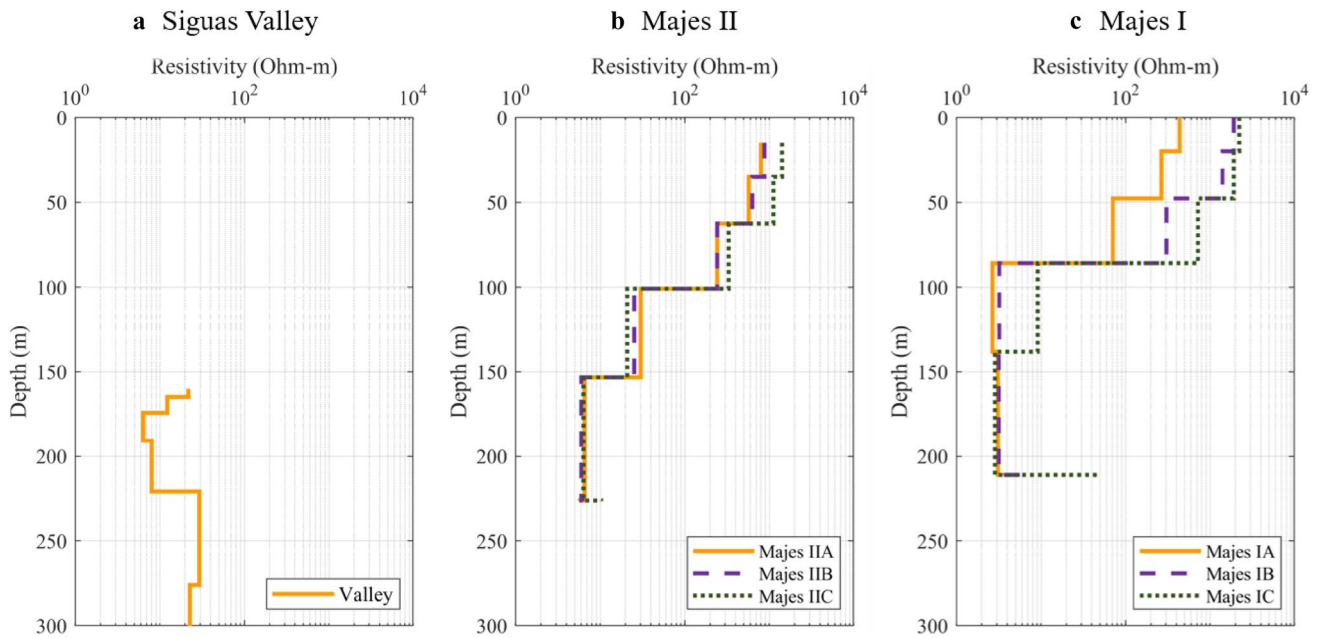


Fig. 7 Geophysical inversion results for the transient electromagnetic (TEM) soundings **a** along the floor of the San Juan De Sigvas Valley, **b** at Majes II, and **c** at Majes I. Station locations are shown in Fig. 5.

Depths are measured with reference to the average elevation of the Majes I survey line

full water saturation. Majes IC, however, is more similar to Majes II soundings, with a resistivity of ~ 9 Ohm-m between 85 and 135 m depth, which likely reflects partial saturation.

Majes IC is located at a nonutilized area of Majes I and thus Majes IC conditions are expected to more broadly resemble those at Majes II.

Seismic surveys

The three lines of 2D seismic data were processed in the Reveal software package in a consistent processing flow, which was developed based on our land data processing experience and tailored to the particular geological environment: (1) geometry assignment; (2) shot statics; (3) trace editing; (4) anomalous amplitude attenuation; (5) ground roll attenuation; (6) refraction mute; (7) stack velocity analysis; (8) zero-offset stack; (9) post-stack time migration; (10) time-to-depth conversion; and (11) post-stack noise attenuation.

The 2D seismic data acquired at Majes I and Majes II are of marginal quality, noisy, and feature overwhelming refracted and surface-wave energy. Weak seismic reflections are visible on some shot gathers but are seldom traceable between gathers. These low-quality data are largely related to the challenges of the improvised weight drop. Because of the variable rock positioning when being dropped, it was difficult to obtain accurate estimates of the “time zero” on which seismic reflection processing is based. The variable impact of the rock with the ground leads to different coupling with each source activation and generates seismic shot gathers with poor repeatability and significantly variable spectra. Ideally, numerous source activations would occur at each shot point, which leads to an increase in the signal-to-noise ratio (S/N); however, due to the time required per shot (approximately 60 s) and the aforementioned issues, the majority of the acquisition involved single shot points. This leads to significant challenges when devising and implementing a seismic reflection processing and imaging strategy.

The final seismic image from the data acquired at Majes II is shown in Fig. 8, with the region of highest data quality denoted by the blue rectangle. The data from Majes II are of somewhat higher quality than Majes I due to the undisturbed near-surface environment. In addition to the strong reflector between 40 and 55 m depth, there are other possible

discontinuities at approximately 70–90 m and a dipping feature between 140 and 160 m depth. However, the interpretation is considered to have a high degree of uncertainty due to the challenges of picking accurate stacking velocities in processing step (7). While the seismic result at Majes II shows promise for imaging the geology, the data are considered of low quality due to challenges associated with the improvised source, and the method should be considered for future surveys with a traditional seismic source.

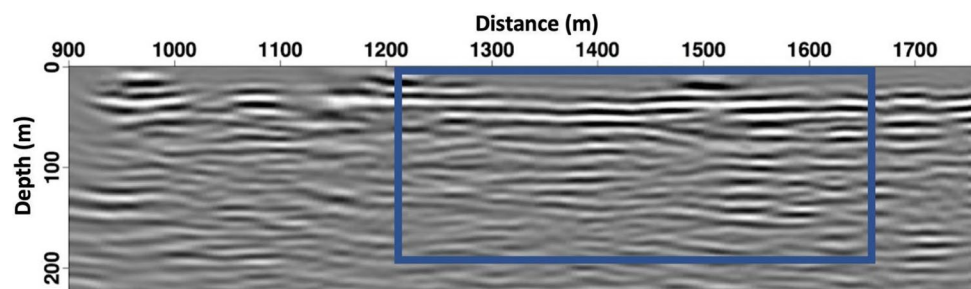
Updated geologic model and water table

We integrate our results from the DC resistivity and TEM surveys to update the geologic model for the area with the water table beneath Majes I (Fig. 9). In the first panel, Majes I TEM inversions and a section of the Majes I DC resistivity model close to the edge of the Sigvas Valley are projected onto the valley wall beneath Majes I. The alignment of the TEM, DC resistivity, geology and water presence is stark, particularly at the Millo/Moquegua contact and top of partially saturated rock near 85 m depth. In the third panel, a subsection of the reflection seismic image shows potential correlation with the DC resistivity and TEM results. In particular, the reflection seismic image indicates reflectivity at 40–55 m depth, as well as evidence for other reflectors at 70–90 m and deeper between 140 and 160 m (Fig. 9c). In the middle panel, the stratigraphic section and water table are updated. Within the Millo formation, the ignimbritic tuff observed discontinuously along the valley wall is not identifiable in the geophysical data along the two survey lines and is possibly not present beneath those locations. The Upper and Lower Moquegua formations have been combined, as the boundary between the two is not clear from the current geophysical data.

Landslide modeling

We use our updated hydrogeologic and geologic data as inputs for modeling the El Zarzal landslide. We perform a suite of finite-element method (FEM) models for El Zarzal to evaluate the influence of agricultural irrigation on initial

Fig. 8 Reflection seismic image from Majes II with the area of highest data quality denoted by the blue rectangle. The location of the survey line is illustrated in Fig. 5



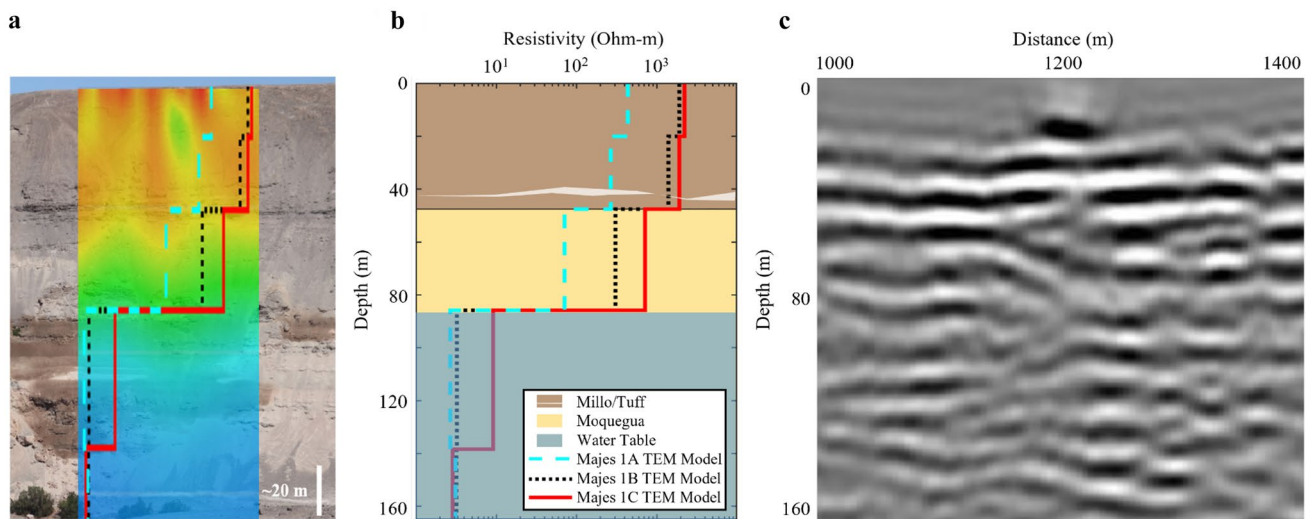


Fig. 9 Updated geologic model beneath Majes. **a** Projection of a section of the DC resistivity model near the edge of the Siguas Valley and the TEM models onto the valley wall beneath Majes I. **b** Refined depths for the Millo/Moquegua contact and top of the water table at

Majes I. **c** Subsection of the reflection seismic image from Majes II containing potential reflectors at depths similar to updated formation contacts determined by DC resistivity and TEM results

failure, and to help inform discussions on possible mitigation at Majes I and prevention at Majes II. The landslide modeling is performed with the RS2 finite-element modeling package (Rocscience 2021). Model strength parameters were determined based on prior studies in the region, representative literature values, and back-calculation from our FEM models (Table 1) (Graber et al. 2020, 2021). All models used the generalized Hoek–Brown strength criterion and all materials were assumed to have a porosity value of 20%. For the lithologies present in the slope, this value is within published typical porosity ranges for sandstones and conglomerates (Manger 1963) and unwelded

tufts (Smyth and Sharp 2006). We used the shear strength reduction (SSR) method to determine the critical strength reduction factor (SRF) [mathematically equivalent to the factor of safety (FS)]. Topography for the models was determined from a 2 m resolution DEM survey (Lacroix et al. 2019). Model boundary elements are constrained in *x* and *y* (pins) along the model base, and in the *x* direction along the model sides (rollers). Boundary elements are free along the upper surface to allow the model topography to deform. With this model approach, we determined the SRF for four scenarios of interest:

Table 1 Summary of material strength values used for model units (values from Graber et al. 2020)

Parameter	Millo Fm	Tuff	Moquegua Fm
UCS (MPa)	1.1	3.5	3.15
Hoek–Brown intact rock constant, m_i	21	13	17
Intact elastic modulus (MPa)	16,500	5500	37,000
Unit weight (dry, MN/m ³)	0.022	0.016	0.027
Poisson’s ratio	0.25	0.2	0.25
–	Peak/Residual	Peak/Residual	Peak/Residual
Geological strength index (GSI)	30/12	40/15	40/10
m_b	1.724/0.906	1.525/0.625	1.994/0.683
s	0.0004189/0.0000567	0.0012726/0.0000791	0.0012726/0.0000454
a	0.5223/0.5747	0.5114/0.5611	0.5114/0.5854
Calculated rockmass modulus (MPa)	1342.8/537.4	878.1/200.5	5907.1/1128.6

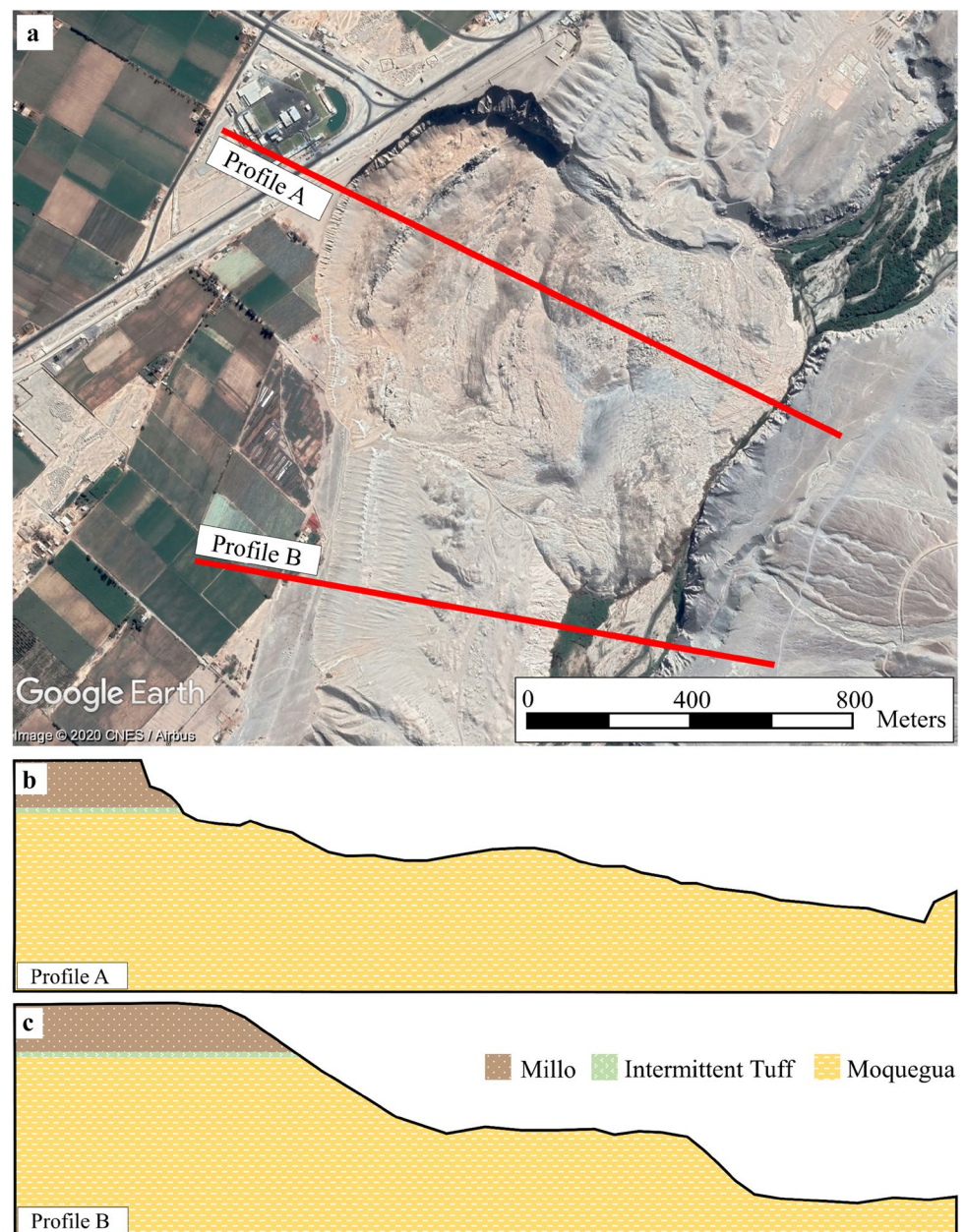
The parameters m_b , s , and a are Hoek–Brown rockmass strength parameters that are calculated using GSI, the Hoek–Brown intact rock constant, and a disturbance factor (Hoek et al. 2002)

1. Historic topography of El Zarzal prior to initial failure and without water present within the Moquegua Formation;
2. Historic topography of El Zarzal prior to initial failure and with water present within the Moquegua Formation;
3. Current topography of El Zarzal, consistent in time with the geophysical surveys, and with water present; and
4. Current topography at El Zarzal and without water present.

The first model was used to assess the stability of El Zarzal prior to irrigation at Majes I. It is important to note

that historical topography at El Zarzal prior to initial failure is not available. As such, we opted to extract a topographic profile immediately to the south of El Zarzal from the current DEM (Fig. 10a) and use these data as a proxy for the historical, pre-failure topography. Figure 10b, c illustrates the current and historical topographies for El Zarzal, respectively. The second model was run to determine if the predicted failure is consistent with historical observations, specifically initiation at the foot of the slope. The third scenario further validates the landslide modeling by comparing predicted slip and current observations, which is failure at the crown of the slide. The fourth model is to understand if the current progression

Fig. 10 Schematic representations of geologic and topographic models used for landslide modeling. **a** Aerial view of the profiles used for landslide modeling. **b** Profile A represents the current topography of El Zarzal slide. **c** Profile B is an estimation of El Zarzal slope geometry prior to the initiation of landslide activity in 2005. Image taken from July 8, 2019 Google Earth repository



of El Zarzal landslide with a near-vertical headscarp will continue toward the Pan-American Highway and GLO-RIA dairy facility even if irrigation at Majes I were immediately shut down.

The results for the four landslide models are presented in Fig. 11 as a set of 2D distributions of shear strain and calculated Critical SRF, which is defined as the ratio of the forces driving failure to the forces resisting failure. When a critical SRF less than 1.0 is observed, failure should occur. Fig. 11b, representing historic topography at El Zarzal without water, shows maximum strain build-up along the foot of the slide and a critical SRF of 1.1. The results indicate that the slope is stable prior to the onset of irrigation. When irrigation water infiltrates and raises the water table, the slope stability decreases, and we predict failure (critical SRF less than 1.0) starting at the lower slope (Fig. 11a). Modeling shows a retrogressive failure pattern matching historical observations of El Zarzal landslide's initiation and progression. The critical SRF for the current topography remains less than 1.0 regardless of the presence of water (Fig. 11c, d). Modeling also highlights that shear strain is highest along the headscarp, the current location of frequent landslide activity. These modeling results suggest that current failure along the scarp of El Zarzal landslide is independent of irrigation. Landslide activity may continue until the slope reaches an angle of repose or encounters a stronger, more competent rock unit or structure.

Discussion

Based on our geophysical surveying at Majes I and planned site of Majes II, we discuss results on: (1) updated geological model beneath Majes I and Majes II sites; (2) identifying the local water table beneath Majes I; (3) modeling different El Zarzal landslide scenarios; (4) identifying appropriate geophysical techniques for planned survey expansion at the site; and (5) recommending options for possible landslide mitigation at Majes I and prevention at Majes II.

Updating the geological model at Majes

The geologic history and stratigraphic column at Majes are relatively well understood, and with the exception of identifying the distinction between Upper and Lower Moquegua, are consistent with what we interpret from the geophysical surveys. The geophysical results, specifically the TEM and resistivity surveys, delineate the major geologic sequences as seen from results at Majes II. Seismic investigations offered only a minor contribution to the updated geologic model due to challenges from the improvised weight source. The geology at Majes can be described as a layer-cake stratigraphy with relatively constant thickness for each of the formations. The geologic model for the site has been updated such that the poorly consolidated conglomerates of the Millo Formation extend to a depth of approximately 50 m beneath the pampa surface. Within the Millo Formation, the discontinuous ignimbritic tuff visible along the valley wall is not

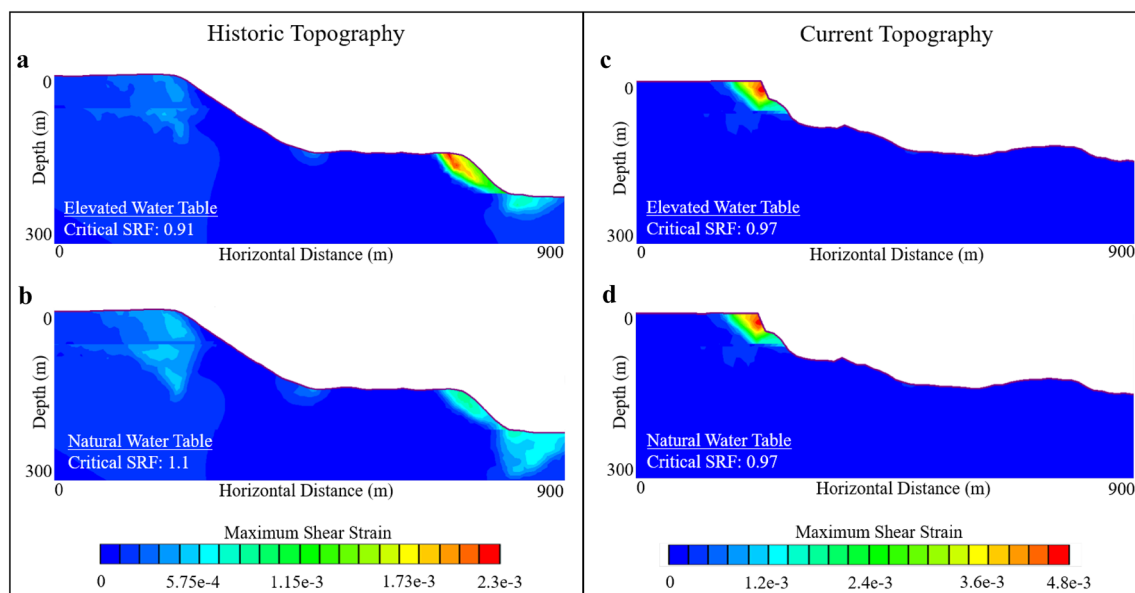


Fig. 11 Maximum shear–strain moduli from landslide modeling of the proxy historical and current topography of El Zarzal landslide. **a** Proxy pre-slide topography with artificially raised water table from

irrigation. **b** Proxy pre-slide topography with natural water table. **c** Current topography with artificially raised water table from irrigation. **d** Current topography with natural water table

clearly defined in the geophysical data, or equally likely, is not present beneath the two survey lines. While the boundary between the Millo and Upper Moquegua Formations is observed in the geophysical data, the transition from Upper to Lower Moquegua Formations are not clear in the current electrical and electromagnetic data. Finally, TEM soundings on the valley floor indicate that the basement is at a depth of approximately 220 m beneath the pampa surface at Majes I.

Identifying the local water table

Based on our TEM and DC resistivity geophysical data, we interpret that the natural water table beneath Majes I and II is approximately 140–150 m below the pampas. The change in conductivity observed beneath Majes I suggests that there is a significant amount of irrigation water infiltrating the subsurface, increasing the elevation of the local water table to approximately 85 m below the surface at locations Majes IA and IB. Near the cliff at Majes I, intermittent moisture along the north–west face of the Sigwas Valley wall is consistent with our resistivity-based interpretations of a partially saturated layer 85–145 m depth below the top of the Pampa de Majes at location Majes IC. The current geophysical data from above the pampas do not image deep enough to determine the depth extent of the aquifer. We recommend future surveys be performed to include updated TEM soundings with the ABEM WalkTEM booster that will increase the depth of investigation to at least 250 m beneath the Pampa de Majes.

Modeling El Zarzal landslide

Geophysical interpretation of the geologic sequences and water table beneath Majes, combined with mechanical properties from previous studies and modeling at the site, allow for modeling El Zarzal landslide. The modeling with a proxy for pre-slide topography (i.e., prior to Majes development) predicts that the valley wall at El Zarzal would be stable in the absence of a water table increase due to agricultural irrigation. In contrast, failure will occur in the presence of a rising water table, consistent with the history of the landslide's progression. Modeling additionally indicates that once irrigation waters saturate the system, retrogressive failure begins at the lower slope near the valley floor, whereas later landslide activity (using current topography) is focused at the headscarp. These modeling results are consistent with the evolution of failure at El Zarzal. Finally, the landslide model predicts that the critical SRF calculated at El Zarzal with current topography no longer depends on the water table. As such, it is likely that El Zarzal will continue to fail and progress into Majes I, regardless of irrigation activity, until reaching a stronger structure/rock unit or achieving the angle of repose.

Recommended geophysical surveys for expanded studies

The current phase of geophysical investigations at Majes I, Majes II, and along the Sigwas Valley floor included 2D seismic, DC resistivity and a collection of TEM soundings. TEM is logistically the simplest and fastest method to perform in and around Majes with as few as one person (and a vehicle). The TEM-based interpretations for the geology and water table are consistent to those of the DC resistivity surveys. The challenge with the TEM analysis at Majes I is that data are sparse and many stations are required for 3D interpretation. The pace of these surveys allows for such an expansion; however, the number and distribution ultimately depends on landowner permissions (permits) to perform these soundings within their fields. DC resistivity performed well at Majes I and Majes II and should be considered for expanded investigations in the future. The data take longer to acquire and are less “sharp” than the TEM inversions; however, with the inherent increase in data density along the 64-electrode dipole–dipole profiles, a continuous subsurface representation is quickly recovered. The seismic surveys faced an insurmountable hurdle after losing our controlled energy source to customs. While our improvised weight drop (a tractor and large boulder) generated a significant amount of seismic energy with weak reflections visible on shot gathers, the associated reflections were seldom coherent between gathers. Regardless, the results proved promising for seismic at Majes to detect geologic features, and the method should be attempted again for future surveys with a more conventional seismic source, perhaps purchased or rented locally if possible.

Options for possible mitigation and prevention of landslides

Results of the current geophysical study and landslide modeling, combined with recent hydrologic analysis of the area (Wei et al. 2021), consistently support the conclusion that inefficient irrigation practices at Majes raised the water table and increased landslide activity. Potential mitigation at Majes I and prevention at the proposed Majes II development should start with efficient irrigation practices at two levels. The first is through decreased use of flood and sprinkler irrigation, and increased use of drip irrigation that maintains higher levels of moisture in the root zone and reduces the rate of infiltration (Wei et al. 2021; Parajuli et al. 2013). The second is through the addition of highly efficient soil ameliorants, such as retaining polymers and biochar (Garcia-Chevesich et al. 2021). Polymers, for example, have the potential to decrease agricultural water usage up to 90% while improving soil conditions and crop productivity (Islam et al. 2011). Remediation at El Zarzal may not

be feasible based on the landslide modeling conclusion that failure may continue at this stage whether or not subsurface water is present. In this case, a thorough geotechnical analysis of the area needs to be performed for the consideration of engineering options, such as retaining walls and shotcrete.

Conclusions

The Majes agricultural development in southern Peru is important for food supply and economic development. While the value for the community is large, recent history indicates that the nexus of agricultural irrigation and geology at Majes may ultimately have the combined effect of destroying agricultural fields along the pampas and valley floors, disrupting flow of the Siguas River, polluting downstream waters, and eliminating a section of the Pan American Highway and the GLORIA dairy facility. We performed a focused set of geophysical studies at Majes to update the geologic structure of the region in the absence of irrigation activities (Majes II) and to define the water table increase due to irrigation (Majes I). The results, incorporated into pre- and post-slip modeling for El Zarzal landslide, support the conclusion that irrigation water accumulating within the Moquegua Formation contributed to initial failure and continued progression of the landslide. To prevent such outcomes at the future Majes II site, the development should implement efficient irrigation practices, such as increasing the use of drip irrigation, eliminating flood and sprinkler irrigation, and incorporating soil ameliorants, such as retaining polymers and biochar that hold the water near the roots while significantly decreasing water usage.

Supplementary Information The online version contains supplementary material available at <https://doi.org/10.1007/s12665-022-10382-0>.

Acknowledgements This work was funded by the Center for Mining Sustainability, a joint venture between the Universidad Nacional de San Agustín de Arequipa (Peru) and the Colorado School of Mines (USA). The authors thank the valuable contributions from the Center for Mining Sustainability, Arequipa, Peru. We thank from Mines: Gavin Wilson, Michael Field, Brian Passerella, Andrei Swidinsky, Michelle Szobody, Debra Marrufo, Paul Santi, Alicia Polo y La Borda Cavero. We thank from UNSA: Alberto Apaza Chino, Joel Gárate Pareja, Jonathan Pilco Sullca, Sergio Pariapaza Quispe. We additionally thank Ricardo Pelaez from SGA Geofísica; Ben Bloss and Michael Pace from the U.S. Geological Survey; Morgan Sander-Olhoef of Guideline Geo; Stephen Cuttler.

Funding This work was funded by the Center for Mining Sustainability, a joint venture between the Universidad Nacional San Agustín (Arequipa, Peru) and Colorado School of Mines (USA).

Availability of data and materials Not applicable.

Code availability Not applicable.

Declarations

Conflict of interest The authors have no conflicts of interest to declare.

Open Access This article is licensed under a Creative Commons Attribution 4.0 International License, which permits use, sharing, adaptation, distribution and reproduction in any medium or format, as long as you give appropriate credit to the original author(s) and the source, provide a link to the Creative Commons licence, and indicate if changes were made. The images or other third party material in this article are included in the article's Creative Commons licence, unless indicated otherwise in a credit line to the material. If material is not included in the article's Creative Commons licence and your intended use is not permitted by statutory regulation or exceeds the permitted use, you will need to obtain permission directly from the copyright holder. To view a copy of this licence, visit <http://creativecommons.org/licenses/by/4.0/>.

References

- AGS (2021) Aarhus GeoSoftware brochure: SPIA TEM and VES Inversion Software. https://ags-cloud.dk/AGS/Product%20Brochures/Aarhus_SPIA.pdf. Last viewed: 11 May 2021
- Ali J, Nizami A, Hebinck P (2017) Mismanagement of irrigation water and landslides in Yourjogh, Pakistan. *Mt Res Dev* 37(2):170–178
- Araujo-Huamán EE, Taipe-Maquerhua EL, Miranda-Cruz R, Valderama-Murillo PA (2017) Dinámica y Monitoreo del Deslizamiento de Siguas; Región Arequipa, istema Caylloma y Arequipa, distrito Majes y San Juan de Siguas. Instituto Geológico, Minero y Metalúrgico, Lima
- Auken E, Christiansen AV (2004) Layered and laterally constrained 2D inversion of resistivity data. *Geophysics* 69(3):752–761
- Best M, Bobrowsky P, Douma M, Carlotto V, Pari W (2009) Geophysical surveys at Machu Picchu, Peru: results for landslide hazard investigations. In: Sassa K, Canuti P (eds) *Landslides—disaster risk reduction*. Springer, Berlin. https://doi.org/10.1007/978-3-540-69970-5_16
- Bradley K, Mallick R, Andikagumi H, Hubbard J, Meilianda E, Switzer A, Hill EM (2019) Earthquake-triggered 2018 Palu Valley landslides enabled by wet rice cultivation. *Nat Geosci* 12(11):935–939
- Carbajal FA (2019) Análisis de vulnerabilidad istemal por deslizamiento en la microcuenca del río Tabarcia, Cantón de Mora, República de Costa Rica. Master's Thesis, Facultad de Geología, Universidad de Costa Rica, Costa Rica
- Chambers J, Meldrum P, Gunn D, Wilkinson P, Merritt A, Murphy W, West J, Kuras O, Haslam E, Hobbs P, Pennington C, Munro C (2011) Geophysical–geotechnical sensor networks for landslide monitoring. In: *Proceedings of the second world landslide forum*, October 2011
- Clague JJ, Evans SG (2003) Geologic framework of large historic landslides in Thompson River Valley, British Columbia. *Environ Eng Geosci* 9(3):201–212
- Dong Y, Jia J, Zhang MS, Sun PP, Zhu LF, Bi JB (2013) An analysis of the inducing effects of irrigation and the responses of loess landslides in Heifangtai area. *Geol Bull China* 32(6):893–898
- Flamme HE, Sirota D, Krahenbuhl R, Li Y, Dugan B, Shragge J, Minaya Lizárraga A (2020) Geophysical investigation to understand local geology and agricultural water movement in relation to landslide activity in Majes, Peru. In: *SEG technical program expanded abstracts 2020*. Society of Exploration Geophysicists, pp 3341–3345
- García-Chevesich P, Wei X, Ticona J, Martínez G, Zea J, García V, Krahenbuhl R (2021) The impact of agricultural irrigation on

- landslide triggering: a review from Chinese, English, and Spanish literature. *Water* 13(1):10
- Gobierno Regional Arequipa (2016) Proyecto Especial Majes Siguas—Autodema. https://www.regionarequipa.gob.pe/Cms_Data/Contenets/GobRegionalArequipaInv/Media/ParticipacionCiudadana.PresupuestoParticipativo/2017/EXPOSICIONES/sitauacion-demajes-siguas-avances-y-beneficios.pdf. Last viewed: 11 May 2021
- Gorokhovich Y, Doocy S, Walyawula F, Muwanga A, Nardi F (2012) Landslides in Bududa, Eastern Uganda: preliminary assessment and proposed solutions. In: Margottini C, Canuti P, Sassa K (eds) *Landslide science and practice. Volume 4: global environmental change*. Springer, Berlin, pp 145–149
- Graber A, Santi P, Radach K, Meza Arestegui P, Chacon Arcaya S (2020) Finite element model calibration in the context of limited data and limited access: a case study from a large landslide in Southern Peru. In: 54th US rock mechanics/geomechanics symposium. American Rock Mechanics Association
- Graber A, Santi P, Meza Arestegui P (2021) Constraining the critical groundwater conditions for initiation of large, irrigation-induced landslides, Siguas River Valley, Peru. *Landslides* 18(12):3753–3767
- Helmstetter A, Garambois S (2010) Seismic monitoring of Séchillienne rockslide (French Alps): analysis of seismic signals and their correlation with rainfalls. *J Geophys Res Earth Surf* 115(F0316)
- Hoek E, Carranza-Torres C, Corkum B (2002) Hoek–Brown failure criterion—2002 edition. In: *Proceedings of the NARMS-TAC conference*, Toronto, 7–10 July 2002, vol 1, pp 267–273
- Huanca A (2011) Actualización de Asignación de Agua En Bloques Pampa de Majes—Arequipa. Autoridad Nacional del Agua, Ministerio de Agricultura, Arequipa, p 849
- Hussain Y, Cardenas-Soto M, Martino S, Moreira C, Borges W, Hamza O, Martinez-Carvajal H (2019) Multiple geophysical techniques for investigation and monitoring of Sobradinho landslide, Brazil. *Sustainability* 11(23):6672
- Ishihara K, Okusa S, Oyagi N, Ischuk A (1990) Liquefaction-induced flow slide in the collapsible loess deposit in Soviet Tajik. *Soils Found* 30(4):73–89
- Islam MR, Hu Y, Mao S, Mao J, Eneji AE, Xue X (2011) Effectiveness of a water-saving super-absorbent polymer in soil water conservation for corn (*Zea mays* L.) based on eco-physiological parameters. *J Sci Food Agric* 91(11):1998–2005. <https://doi.org/10.1002/jsfa.4408>
- Jin YL, Dai FC (2007) The mechanism of irrigation-induced landslides of loess. *Chin J Geotech Eng* 29(10):1493–1499
- Jurio EM, Chimenton ME, Mare MD (2014) Desestabilización del istema natural a partir de cambios en el uso del suelo: El caso de los deslizamientos de Vista Alegre, Provincia del Neuquén. *Boletín Geofísico* 36:11–25
- Knott JR (2008) The influence of irrigation on slope movements, Ventura County, California, USA. *Environ Eng Geosci* 14(3):151–165
- Lacroix P, Araujo G, Hollingsworth J, Taipe E (2019) Self-entrainment motion of a slow-moving landslide inferred from Landsat-8 time series. *J Geophys Res Earth Surf* 124(5):1201–1216
- Lacroix P, Dehecq A, Taipe E (2020) Irrigation-triggered landslides in a Peruvian desert caused by modern intensive farming. *Nat Geosci* 13(1):56–60
- Lee YS, Cheuk CY, Bolton MD (2008) Instability caused by a seepage impediment in layered fill slopes. *Can Geotech J* 45(10):1410–1425
- Mainsant G, Larose E, Brönnimann C, Jongmans D, Michoud C, Jaboyedoff M (2012) Ambient seismic noise monitoring of a clay landslide: toward failure prediction. *J Geophys Res* 117(F01030)
- Manger E (1963) Porosity and bulk density of sedimentary rocks. US Geological Survey, Bulletin 1144-E
- Meza Arestegui P, Chacon Arcaya S (2017) Evaluacion Preliminar de las Condiciones Geodinamicas del Deslizamiento El Zarzal, Alto Siguas. Thesis, Universidad Nacional de San Agustín de Arequipa, Arequipa, Peru
- Oldenburg DW, Li Y (1994) Inversion of induced polarization data. *Geophysics* 59(9):1327–1341
- Oldenburg DW, Li Y (1999) Estimating depth of investigation in dc resistivity and IP surveys. *Geophysics* 64(2):403–416
- Parajuli PB, Jayakody P, Sassenrath GF, Ouyang Y, Pote JW (2013) Assessing the impacts of crop-rotation and tillage on crop yields and sediment yield using a modeling approach. *Agric Water Manag* 119:32–42
- Perrone A, Iannuzzi A, Lapenna V, Lorenzo P, Piscitelli S, Rizzo E, Sdao F (2004) High-resolution electrical imaging of the Varco d’Izzo earthflow (southern Italy). *J Appl Geophys* 56(1):17–29
- Reyes W, Jiménez F, Faustino J, Velásquez S (2006) Vulnerabilidad y Áreas Críticas a Deslizamientos en la Microcuenca del Río Talgua, Honduras. *Recur Nat Ambiente* 48:103–110
- Rocscience (2021) Rocscience product sheet: RS2 2D geotechnical finite element analysis. <https://www.rocscience.com/assets/resources/products/RS2-Product-Sheet.pdf>. Last viewed: 13 May 2021
- Rosales UB, Centeno YC (2009) Vulnerabilidad potencial de los suelos a deslizamientos de tierra en el municipio de La Conquista, Carazo, Nicaragua. Bachelor’s Thesis, Facultad de Recursos Naturales y del Ambiente, Universidad Nacional Agraria, Managua, Nicaragua
- Smyth RC, Sharp Jr JM (2006) The hydrology of tuffs. In: Heiken G (ed) *Tuffs—their properties, uses, hydrology, and resources*. Geological Society of America special paper 408, pp 91–111
- Soncco Y, Manrique N (2018) Peligro por Deslizamientos en el Sector Matarani, Tacna; Informe Técnico N° 6833; Instituto Minero, Geológico y Metalúrgico: Lima, Peru
- Valderrama P, Araujo GE, Fidel L, Miranda R (2015) Investigación del Deslizamiento de Lari; Primer report; Instituto Minero, Geológico y Metalúrgico, Lima, Peru
- Wei X, Garcia-Chevesich P, Alejo F, García V, Martínez G, Daneshvar F, Bowling LC, Gonzáles E, Krahenbuhl R, McCray JE (2021) Hydrologic analysis of an intensively irrigated area in southern Peru using a crop-field scale framework. *Water* 13(3):318
- Wu W, Wang W, Feng X, Wang N (1999) Prevention countermeasures of geological hazards caused by agricultural irrigation in semi-arid area. *Chin J Geol Hazard Control* 10(4):62–66
- Yadún CA, Guzman J, Aguirre PM (2020) Evaluación de Riesgos Ambientales en la Gestión del Riego en el Canal de San Rafael y Monteolivo, de la Cuenca del Río Escudillas. CUVILLIER VERLAG Press, Göttingen

Publisher's Note Springer Nature remains neutral with regard to jurisdictional claims in published maps and institutional affiliations.